

## Simulation of the Madden–Julian Oscillation in a Coupled General Circulation Model. Part II: The Role of the Basic State

PETER M. INNESS, JULIA M. SLINGO, ERIC GUILYARDI, AND JEFFREY COLE

*NERC Centre for Global Atmospheric Modelling, Department of Meteorology, University of Reading, Reading, United Kingdom*

(Manuscript received 17 January 2002, in final form 15 July 2002)

### ABSTRACT

In Part I of this study it was shown that air–sea coupling had a positive impact on some aspects of the simulation of the Madden–Julian oscillation (MJO) by a GCM. However, errors in the basic-state climate of that GCM appeared to be preventing the MJO-related convection from propagating into the west Pacific. In this paper, the actual impact of these errors will be addressed. An integration of a flux-adjusted version of the coupled model has been performed, which has reduced basic-state errors in the west Pacific. In this version of the coupled GCM the MJO does propagate into the west Pacific. The simulation of the MJO by a coupled model with the same atmospheric component but a different ocean GCM is also analyzed. This coupled GCM has similar systematic errors in low-level zonal wind and precipitation to the model studied in Part I, but with warmer SSTs. Results from this experiment, together with the other available evidence, suggest that it is the errors in the low-level zonal wind component in the west Pacific that prevent the MJO from propagating into this region in the coupled GCM rather than the errors in absolute values of SST.

### 1. Introduction

In Part I of this study (Inness and Slingo 2003, hereafter referred to as IS03) the simulation of the Madden–Julian oscillation (MJO) by a coupled ocean–atmosphere general circulation model (GCM) was examined and compared with MJO simulation by the same atmospheric model without an interactive ocean, and with the observed MJO. Some aspects of the MJO simulation were found to improve when the atmospheric GCM was coupled to an interactive ocean model. In particular, the eastward propagation of enhanced convection across the Indian Ocean occurred in the coupled GCM but not the atmospheric GCM which represented the intraseasonal variability of convection in this region as a standing oscillation. However, it was clear that there were still deficiencies in the representation of the MJO by the coupled GCM. Perhaps the most serious short-coming of the coupled GCM was that while the enhanced convective region propagated eastward across the Indian Ocean, it tended to come to an abrupt halt over the Maritime Continent at a longitude of about 120°E. In fact, only three rather weak MJO events were found to propagate as far east as 150°E in 19 yr of model integration.

It was suggested in IS03 that this lack of extension of the MJO into the west Pacific may be due to errors in the basic state of the coupled GCM. Theories such as that of Flatau et al. (1997) suggest that, if the MJO is a coupled mode, mean westerly surface winds are necessary for the enhanced convective region to move towards the east, and various modeling and observational studies exist to back up this proposal (e.g., Hendon and Glick 1997; Waliser et al. 1999; Woolnough et al. 2000). In the GCM under study, the low-level winds on and just to the south of the equator in the west Pacific are easterly rather than westerly. Hence, if the coupled theory for the MJO of Flatau et al. (1997) is correct, the SST anomalies induced to the east and west of the enhanced convective region will be of the wrong sign, inhibiting further eastward propagation. It is also possible that the lack of extension into the west Pacific in the coupled GCM is because the SSTs in this region are too cold to support large-scale enhanced convection in the coupled model regardless of the surface flux variability.

It is interesting to speculate as to whether the MJO-related convective envelope simulated by the coupled GCM would have continued to propagate toward the east, across the west Pacific warm pool, if the low-level mean winds in this region were westerly. In this Part II of the paper, we will address this question by examining the MJO simulation by a version of the coupled GCM which is run with limited-area flux adjustments in order to correct some of the basic-state errors in the coupled GCM. In section

---

*Corresponding author address:* Dr. Peter Inness, NERC Centre for Global Atmospheric Modelling, Department of Meteorology, University of Reading, P.O. Box 243, Earley Gate, Reading RG6 6BB, United Kingdom.  
E-mail: pete@met.rdg.ac.uk

2 the experimental design will be described. In section 3, the impact of the flux adjustment on the basic state of the coupled GCM will be discussed, and this will be followed by an examination of the MJO simulation in section 4. In section 5, the MJO simulation by a coupled GCM using the same atmospheric component as before, but with a different ocean model will be briefly described. Results will be discussed in section 6.

## 2. Flux-adjusted experiment design

In IS03 it was shown that an atmosphere–ocean coupled GCM—the third Hadley Centre Coupled Ocean–Atmosphere General Circulation Model (HadCM3)—was able to reproduce some aspects of the MJO. HadCM3 has a stable climate and is able to run without the need for heat flux adjustments. The formulation of HadCM3 is described in detail in Gordon et al. (2000), together with a description of its simulation of ocean heat transports and SST. Briefly, the atmospheric component of HadCM3 is a gridpoint model with horizontal spacing of  $2.5^\circ$  latitude  $\times$   $3.75^\circ$  longitude. It is usually run with 19 vertical levels but this was increased to 30 in the experiment described in IS03, following results described by Inness et al. (2001). In an atmosphere-only version of this GCM they showed that increasing the vertical resolution led to an improved representation of the distribution of convective cloud tops in the Tropics in an atmosphere-only simulation with this GCM which may have implications for the simulation of the MJO. Convection is parameterized using the mass-flux scheme of Gregory and Rowntree (1990), with the addition of convective momentum transports (Gregory et al. 1997). The ocean component of HadCM3 has a  $1.25^\circ \times 1.25^\circ$  latitude–longitude grid with 20 vertical levels. The top three levels are all 10 m thick. Horizontal eddy mixing is parameterized using a version of the Gent and McWilliams (1990) adiabatic thickness diffusion scheme. Near-surface vertical mixing is modeled using a combination of a Kraus and Turner (1967) mixed layer submodel and a  $K$ -theory scheme. Coupling between atmosphere and ocean occurs once per day. As discussed by Shinoda and Hendon (1998), it may be important to include the diurnal variation of the surface fluxes to fully capture the intraseasonal variability of SST associated with the MJO. This possibility will be discussed further in section 6.

In order to investigate the sensitivity of the MJO simulation to the basic-state errors in low-level zonal wind and SST described in section 2 of IS03, a flux-adjusted version of HadCM3 has been developed. Although the largest SST errors in HadCM3 are in the extratropical North Pacific, these errors will not be addressed by the flux adjustment as we wish to have as small an impact as possible on the overall basic state of the GCM. As discussed in section 2 of IS03, some of the systematic errors in the equatorial Pacific Ocean in HadCM3 are the result of a coupled feedback mechanism. The con-

vective precipitation over Indonesia is too strong in HadCM3 and this drives an enhanced Walker circulation across the equatorial Pacific with very strong low-level easterly trade winds. These winds in turn drive anomalously strong Ekman divergence in the surface layer of the equatorial Pacific Ocean, forcing upwelling and anomalously cold SSTs, with errors of up to  $3^\circ\text{C}$  on the equator, centered just to the east of the date line. These SST errors lead to an anomalous zonal temperature gradient in the west Pacific and hence a further reduction in the westerly wind component here, reinforcing the systematic error. In order to break this coupled mechanism, we will apply flux adjustments to the equatorial ocean surface in order to weaken the erroneous SST gradient in the west Pacific and thus enhance the low-level westerly wind component to the west of the date line. The flux-adjusted experiment will be referred to as HadCM3-FA.

Some other coupled model experiments have investigated the impact of air–sea interaction on the MJO by using atmospheric GCMs coupled to mixed layer or “slab” ocean models with varying levels of complexity. Hendon (2000) used a rather complex one-dimensional mixed layer model in which the mixed layer depth was able to vary, whereas Waliser et al. (1999) used a much simpler, highly idealized, fixed depth mixed layer model. All such mixed layer models require the ocean temperatures to be relaxed toward observed climatological values in order to account for neglected processes such as horizontal advection. This will introduce a timescale for the SST variability, which is an artifact of the relaxation. If this timescale is chosen to be close to the period on which the SSTs would be expected to vary in association with the MJO then it will be difficult to isolate the “natural” SST variability from that due to the relaxation. By using a full ocean model with horizontal advection processes, and by using flux adjustment to maintain the SSTs close to climatological values, the inclusion of an implicit timescale of SST variability has been avoided. However, it is inevitable that, as well as going some way toward correcting the basic-state errors in HadCM3, the flux-adjustment technique will also introduce other changes to the climatology of the coupled GCM, which may lead to differences from the unadjusted coupled GCM. In general, it would be expected that using flux adjustment should lead to a coupled GCM climatology which is closer to the atmospheric component of that GCM forced by observed SSTs.

### *Implementation of flux adjustments*

Flux adjustments are calculated by running the coupled GCM for 20 yr with the SSTs between  $10^\circ\text{N}$  and  $10^\circ\text{S}$  in the Pacific and Indian Ocean being relaxed back toward climatology on a timescale of approximately 14 days. Between  $5^\circ\text{N}$  and  $5^\circ\text{S}$  the relaxation is applied in full. To the north and south of this strip, the relaxation is linearly ramped down to zero so that north of  $10^\circ\text{N}$

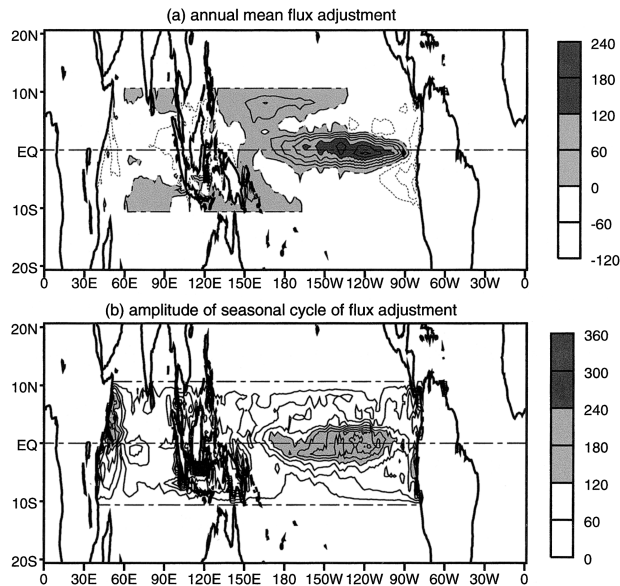


FIG. 1. (a) Annual mean flux adjustment for HadCM3-FA. (b) Amplitude of annual cycle of flux adjustment in HadCM3-FA. Contour interval is  $30 \text{ W m}^{-2}$  in both (a) and (b).

and south of  $10^{\circ}\text{S}$  the SSTs are completely free running. The anomalous fluxes required to achieve this relaxation are saved and an annual cycle of flux adjustments is calculated by averaging the anomalous flux for each month of the year over the 20-yr integration. The model is then run a second time with the relaxation of SSTs switched off, but with the flux adjustment terms applied at the ocean surface. The model calculates daily flux adjustment values by interpolating linearly between the monthly mean values. The initial conditions for this second integration were taken from the end of the integration with the relaxation of SSTs. The model was run with flux adjustments for 20 yr.

The annual mean flux adjustment is shown in Fig. 1a. As would be expected, the fluxes are large and positive (i.e., into the ocean) in the middle of the equatorial cold tongue with a maximum value of  $186 \text{ W m}^{-2}$  at  $120^{\circ}\text{W}$ . In the bulk of the Indian Ocean and west Pacific warm pool region the flux adjustments are much smaller—generally less than  $\pm 30 \text{ W m}^{-2}$ . More importantly, the annual cycle of flux adjustments in this region is also very small so that time variations of the flux adjustments should have very little impact on any intraseasonal variability of SST. The amplitude of the annual cycle of the flux corrections is shown in Fig. 1b. This is calculated very simply by taking the difference between the maximum and minimum flux adjustment term at each grid point. Apart from a few grid points adjacent to the Indonesian islands and along the coast of East Africa, there is very little variation in the flux adjustment through the year to the west of the date line, with the annual variation being generally between 30 and  $60 \text{ W m}^{-2}$ . Observational studies such as that of Zhang and McPhaden (2000) have shown that the amplitude

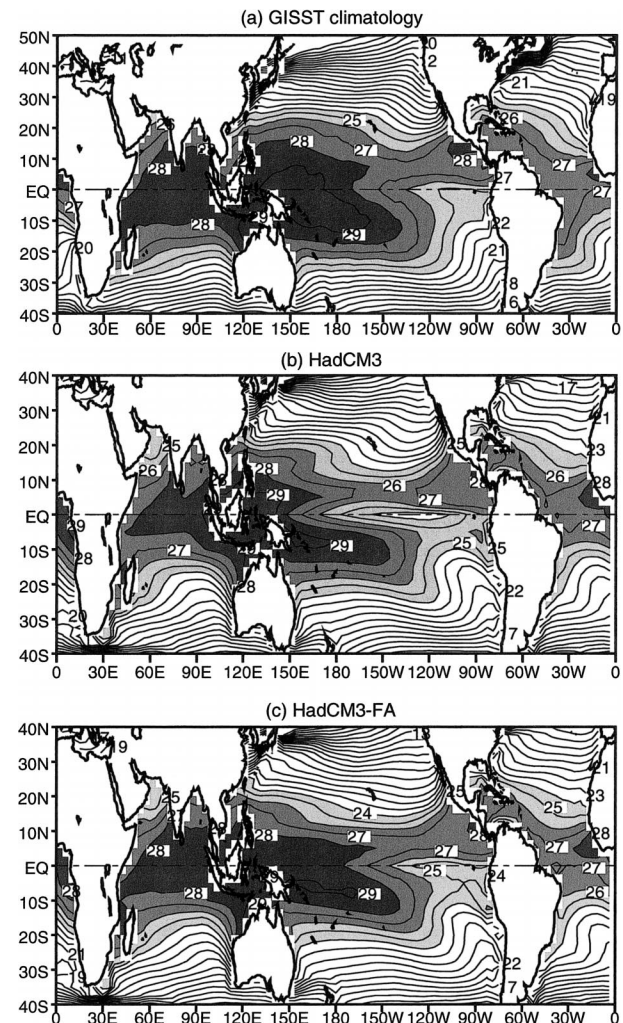


FIG. 2. Oct–Apr SST climatologies from (a) GISST observational dataset (1979–95), (b) 20 yr of HadCM3 simulation, and (c) 20 yr of HadCM3-FA simulation. Contour interval is  $1^{\circ}\text{C}$ .

of intraseasonal variations in net surface flux associated with the MJO are of the order of  $100 \text{ W m}^{-2}$ . Thus we are confident that the implementation of the flux adjustment in the model should not disable the intraseasonal coupling between the ocean and atmosphere, which is the focus of this study.

### 3. Flux-adjusted GCM basic state

The impact of the flux adjustments on the basic state of the coupled GCM is very much as expected. Figures 2, 3, and 4 show the October–April (ONDJFMA) climatologies of SST, precipitation and 850-hPa zonal wind respectively for the two GCM integrations with and without flux adjustment, and for observations. SSTs in the central Pacific are warmer in HadCM3-FA by up to  $3^{\circ}\text{C}$  while, those around Indonesia are slightly cooler. The west Pacific warm pool in HadCM3-FA is now a fairly uniform region of SST in excess of  $28^{\circ}\text{C}$ , whereas

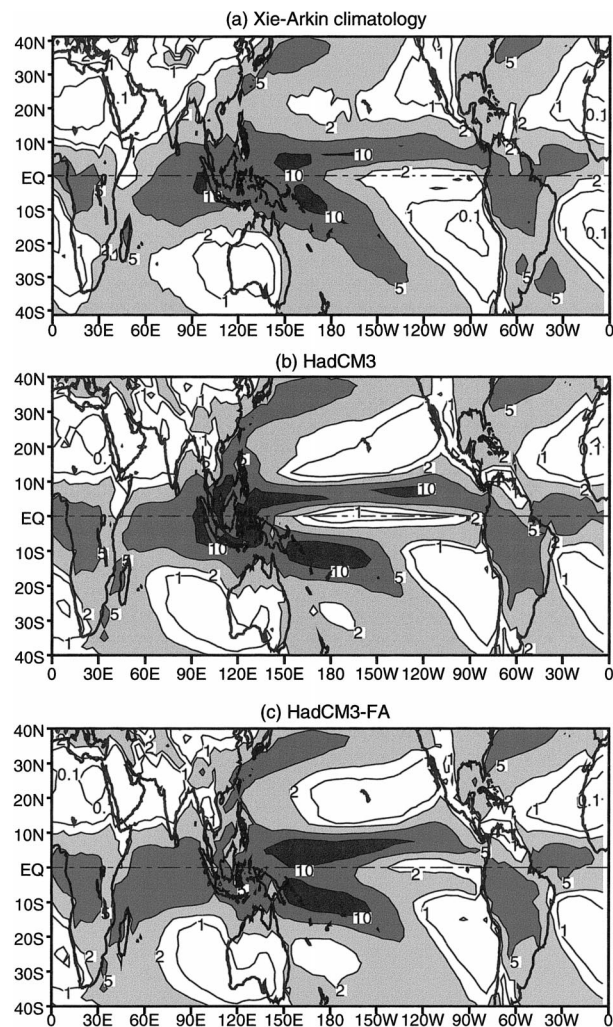


FIG. 3. Oct–Apr precipitation climatologies from (a) the Xie–Arkin observed dataset, (b) 20 yr of HadCM3 simulation, and (c) 20 yr of HadCM3-FA simulation. Contours are at 0.1, 1.0, 2.0, 5.0, and 10.0  $\text{mm day}^{-1}$ .

this region in HadCM3 was dominated by a strong zonal SST gradient. However, because the flux adjustments are only applied between  $10^{\circ}\text{N}$  and  $10^{\circ}\text{S}$ , the strong meridional gradients of SST to the north and south of these latitudes, when compared to the Global Sea Ice and Sea Surface Temperature (GISST) 3.0 climatology (Rayner et al. 1996), are now even stronger in HadCM3-FA.

Tropical precipitation adjusts in line with the SST changes so that the excessive precipitation over the Maritime Continent in HadCM3 is reduced by up to  $10 \text{ mm day}^{-1}$  whereas rainfall increases over a large region of the equatorial western and central Pacific by values in excess of  $5 \text{ mm day}^{-1}$ . The rainfall amounts in the ITCZ in HadCM3-FA are now up to  $5 \text{ mm day}^{-1}$  heavier than the Xie and Arkin (1996) climatology. This is possibly a consequence of the strong meridional SST gradient just to the north of the ITCZ leading to enhanced low-

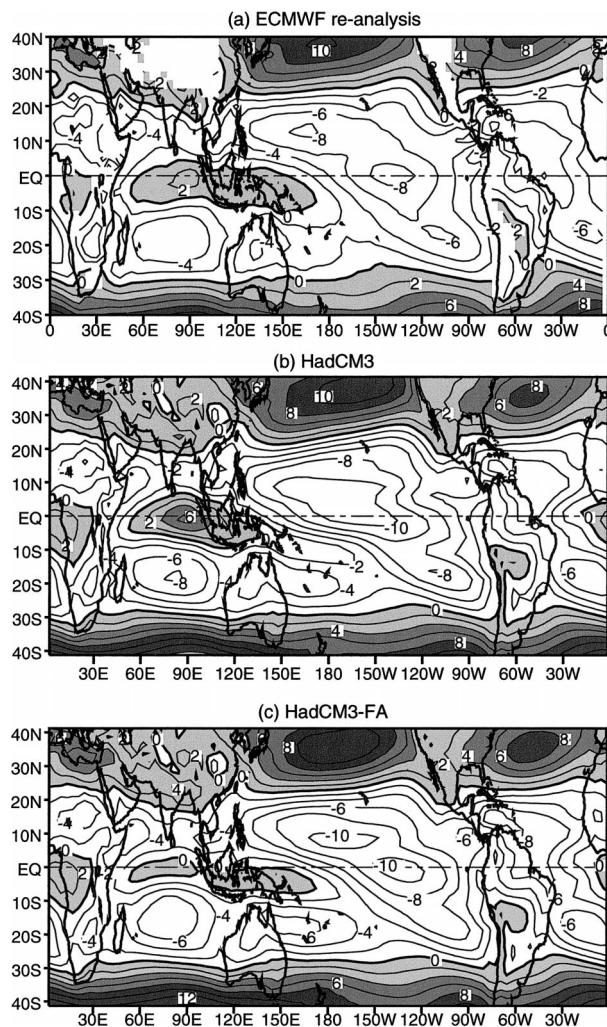


FIG. 4. Oct–Apr 850-hPa zonal wind climatologies from (a) ECMWF reanalyses (1979–93), (b) 20 yr of HadCM3 simulation, and (c) 20 yr of HadCM3-FA simulation. Contour interval is  $2 \text{ m s}^{-1}$ . Regions with westerly winds are shaded.

level meridional convergence. Note also that the rainfall deficit in the east Pacific to the north of the ITCZ in HadCM3 is unaffected by the flux adjustments, consistent with the lack of change of the SST structure here.

Perhaps the most important change from HadCM3 to HadCM3-FA is in the low-level zonal wind field in the warm pool region. The 850-hPa zonal wind component becomes more westerly across the equatorial west Pacific by up to  $6 \text{ m s}^{-1}$ . In the eastern Indian Ocean the westerly flow, which was excessively strong in HadCM3, is reduced to mean values much closer to European Centre for Medium-Range Weather Forecasts (ECMWF) reanalyses (ERA). The strong easterly trade winds in the central Pacific in HadCM3 are reduced slightly in HadCM3-FA but are still about  $2 \text{ m s}^{-1}$  stronger than the reanalysis field. This is consistent with the atmosphere-only version of this GCM forced with observed SST (see IS03) and suggests that this remaining

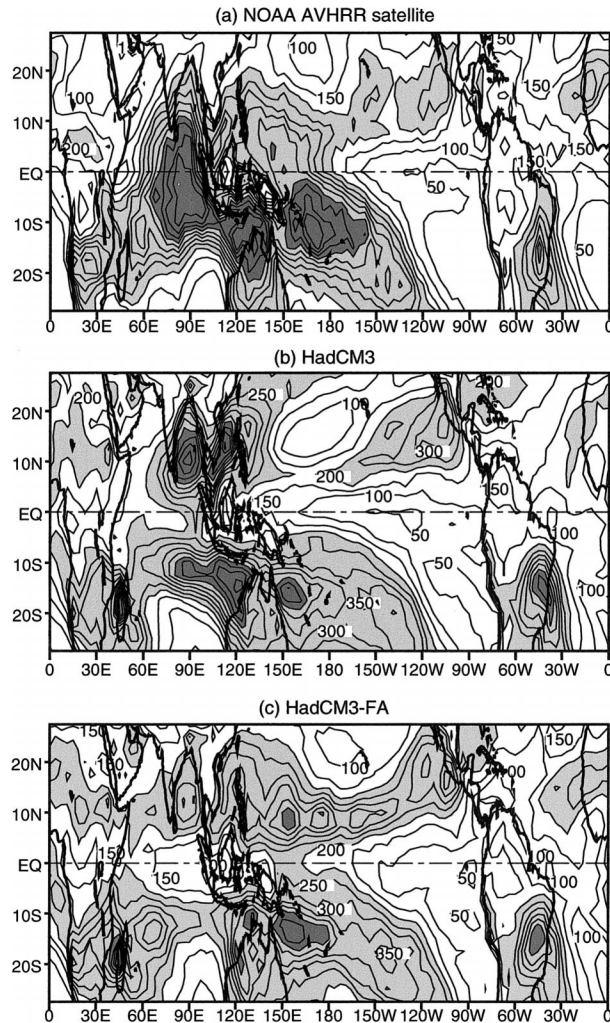


FIG. 5. Variance of 20–100-day bandpass-filtered OLR for the Oct–Apr period from (a) 15 yr of NOAA AVHRR satellite data, (b) 20 yr of HadCM3, and (c) 20 yr of HadCM3-FA. Contour interval is  $50 \text{ (W m}^{-2}\text{)}^2$ .

easterly bias is associated with the atmospheric component of the model. For the purposes of this experiment, the flux adjustment has the desired impact on the basic state of the GCM with the extension of low-level westerly flow into the west Pacific between the equator and  $10^\circ\text{S}$ . This suggests that the MJO itself may propagate further east in this version of the GCM. This will be investigated in the following sections.

#### 4. The MJO in the flux-adjusted GCM

Before looking at diagnostics of MJO activity specifically, it is useful to assess the overall intraseasonal variability of convection in HadCM3-FA. Figure 5 shows the variance of the 20–100-day bandpass-filtered outgoing longwave radiation (OLR) for the October–April period from the National Oceanic and Atmospheric Administration (NOAA) Advanced Very

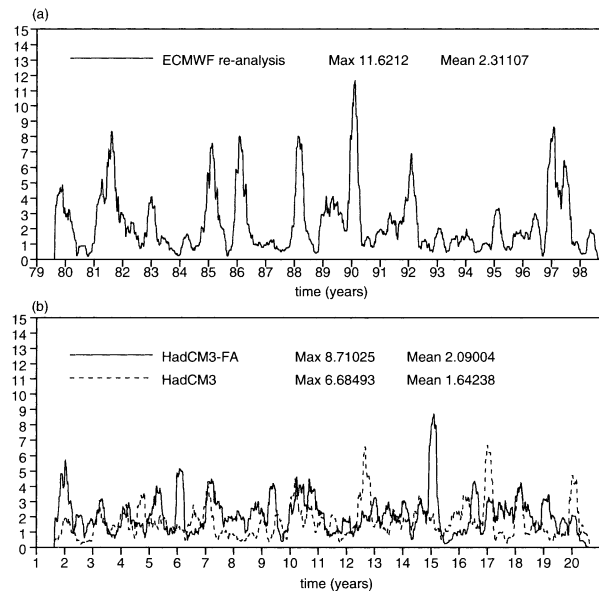


FIG. 6. Time series of an index of MJO activity based on the 20–100-day-filtered variance of 200-hPa zonal wind averaged between  $10^\circ\text{N}$  and  $10^\circ\text{S}$ : (a) ECMWF re-analysis and (b) HadCM3 (dashed line) and HadCM3-FA (solid line). The model time series are displayed on a different time axis than the reanalysis series as the coupled GCM has a 360-day calendar.

High Resolution Radiometer (AVHRR), HadCM3, and HadCM3-FA. While both versions of the coupled model are deficient in variability between  $5^\circ\text{N}$  and  $5^\circ\text{S}$  through the warm pool region, Fig. 5c confirms that the use of flux adjustment in HadCM3-FA has not killed off the intraseasonal variability of convection. HadCM3-FA shows slightly less variability of OLR in the Indian Ocean than HadCM3, but has increased variability in the west Pacific, particularly on, and just to the north of, the equator. The unrealistically high variability of OLR in the Bay of Bengal and South China Sea in HadCM3 has been reduced in HadCM3-FA.

The MJO index of Slingo et al. (1999) described in IS03 can be used as an initial indicator of the strength of the global signal of the MJO. Figure 6 shows this index plotted for 20 years of both the standard and flux-adjusted versions of HadCM3 and for ERA data. Although the mean value of the index from the flux-adjusted run is significantly higher than that from HadCM3, it is still significantly lower than that from the reanalyses. This suggests that the change in the mean state has had little overall impact on the strength of intraseasonal variability in the GCM and that any changes to the MJO simulation will be subtle. The index of both model versions is weaker than the observed index.

The index itself relies on the projection of MJO variability onto the upper-level winds on a global scale. If part of the MJO signal is missing; for instance, if the MJO does not extend into the west Pacific, as was seen for HadCM3 in IS03, the strength of the index will be reduced. The fact that the index is weak for both ver-

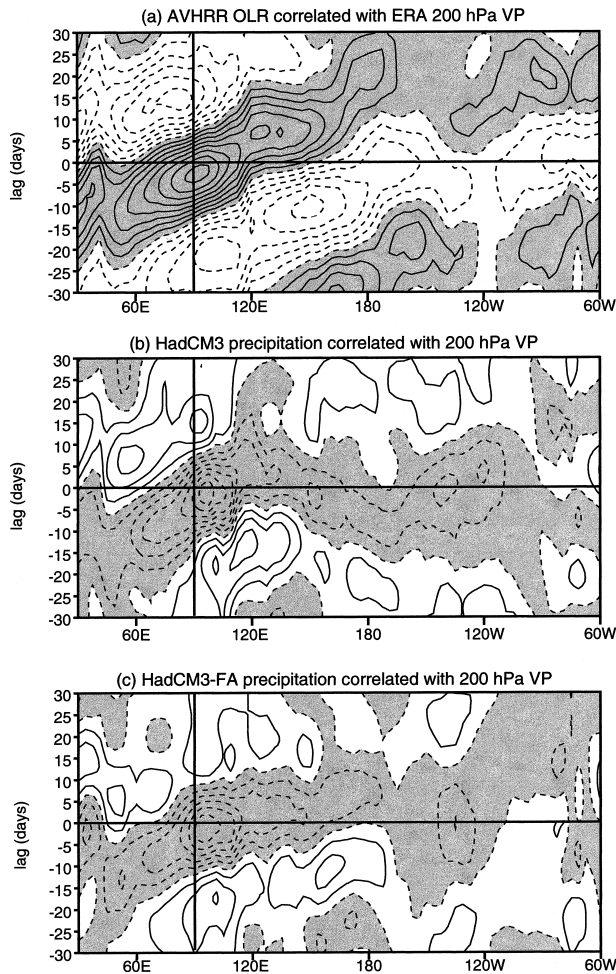


FIG. 7. Lag-correlation plots of OLR or convective precipitation averaged between  $10^{\circ}\text{N}$  and  $10^{\circ}\text{S}$  with 200-hPa velocity potential (VP) at  $90^{\circ}\text{E}$ , also averaged between  $10^{\circ}\text{N}$  and  $10^{\circ}\text{S}$ : (a) NOAA AVHRR OLR correlated with ECMWF reanalysis VP, (b) HadCM3 precipitation and VP, and (c) HadCM3-FA precipitation and VP. Shading indicates negative correlations between precipitation and VP, and positive correlations between OLR and VP. Contour interval is 0.1. All data are 20–100-day bandpass filtered.

sions of the coupled GCM suggests that there may be a similar problem with the MJO not extending into the west Pacific in HadCM3-FA, or perhaps the MJO has been weakened in the Indian Ocean sector. The index does not provide any detail of the structure or propagation characteristics of the MJO and so further analysis is necessary to ascertain the reasons for the similarity of the index in both coupled versions of the GCM.

Differences between the two coupled GCM experiments become apparent when the eastward propagation of convection is examined. Using the same lag-correlation technique as in IS03, Fig. 7 shows the progression of the convective precipitation across the Indo-Pacific region. In HadCM3 there is an abrupt halt to any eastward propagation east of  $120^{\circ}\text{E}$ . In HadCM3-FA, this interruption to the eastward propagation is not apparent.

Although the correlations are still rather weak at longitudes away from the base longitude of  $90^{\circ}\text{E}$ , there is a clear change of behaviour between the two versions suggesting that the MJO convective region does extend into the west Pacific in HadCM3-FA.

The same lag-regression technique used in IS03 has been applied to HadCM3-FA to show the spatial distribution of convective precipitation and 850-hPa winds associated with the MJO. Figure 8 shows these regressions at 6-day intervals and can be compared with Figs. 7, 8, and 9 in IS03 for observations, HadCM3 and the atmosphere-only component of the model, HadAM3. The time lags are relative to a 200-hPa velocity potential minimum at  $90^{\circ}\text{E}$  on the equator. In the Indian Ocean, the pattern of enhanced convection developing in the west and propagating eastward between day  $-18$  and day 0 is qualitatively similar between HadCM3 and HadCM3-FA, although the magnitude of the anomaly is weaker in HadCM3-FA. However, between days 0 and  $+6$ , the enhanced convection in HadCM3-FA propagates into the west Pacific. In HadCM3, the enhanced convective region split into two centers as it approached Indonesia, with the northern center moving into the South China Sea and the southern center propagating into the South Pacific convergence zone (SPCZ). Positive convective anomalies in the Pacific in HadCM3 were the result of the almost instantaneous flaring of convection right along the ITCZ and were not associated with eastward propagation. In contrast, the HadCM3-FA convective centre shows much less evidence of splitting. The enhanced convection in HadCM3-FA moves into the SPCZ by day  $+12$ . It is also noticeable that the westerly wind anomaly also propagates into the equatorial west Pacific at around day  $+12$ , whereas in HadCM3, the wind anomaly split into two following the convection, with one branch centered around  $10^{\circ}\text{N}$  and the other to the south of  $10^{\circ}\text{S}$ .

#### a. Relationship between convection, surface fluxes, and SST

The different behavior of the MJO convection in the standard and flux-adjusted versions of HadCM3 is further highlighted by studying the lag correlations between convection, SST and surface fluxes. Figure 9 shows these relationships for SST, surface shortwave flux (SWF), surface latent heat flux (LHF), and also the lag correlation between LHF and surface zonal wind stress (UST). This figure can be directly compared with Figs. 10 and 11 of IS03 which show the same plots for ERA reanalyses and the standard version of HadCM3. In all these plots, fluxes are taken to be positive *into* the ocean surface, so that a positive LHF anomaly is due to reduced evaporation.

In the standard version of HadCM3, the lead-lag relationship between convective precipitation and SST becomes rather weak to the east of  $140^{\circ}\text{E}$ , with correlations

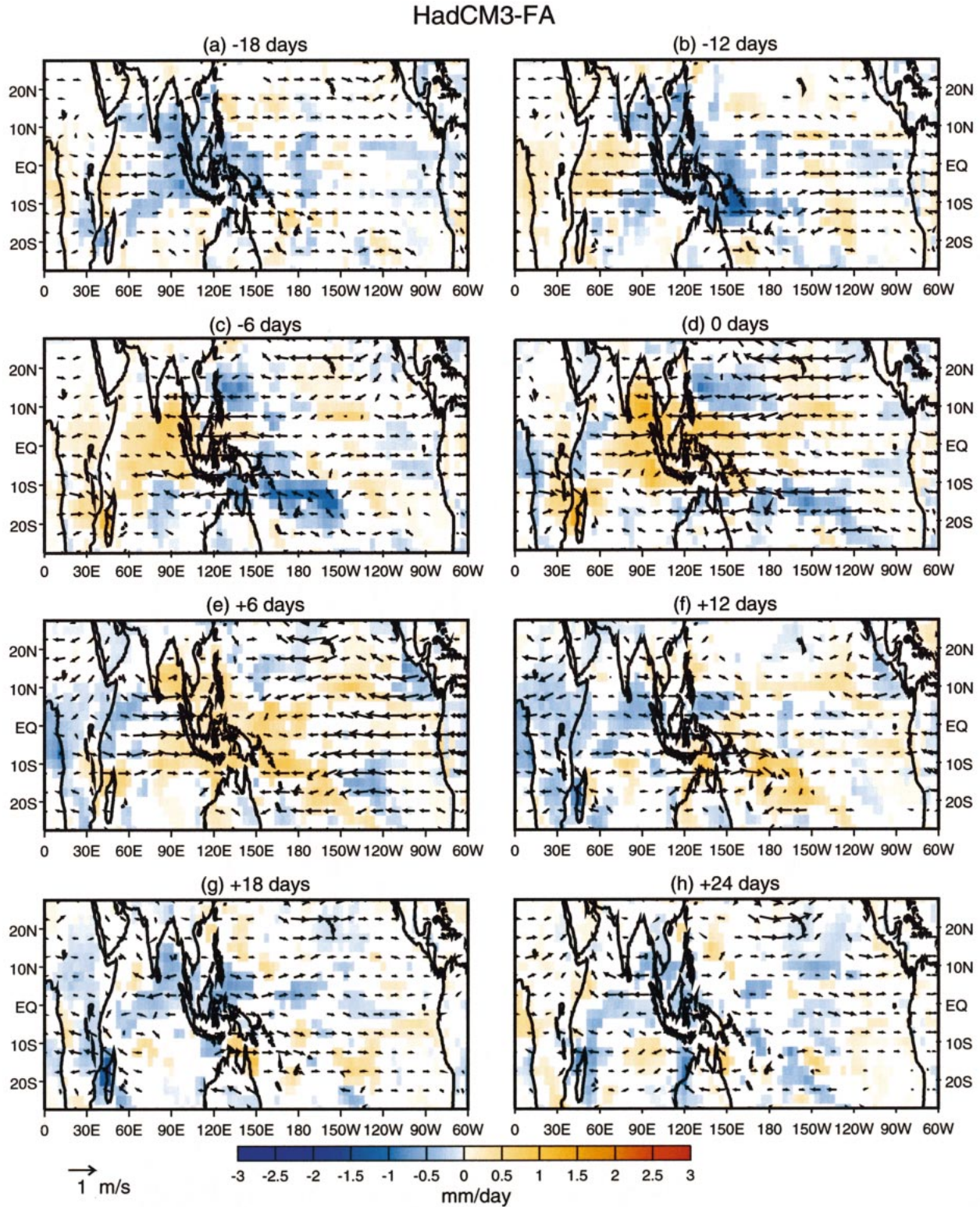


FIG. 8. Lag regressions of convective precipitation onto a base time series of 20–100-day filtered 200-hPa velocity potential at 90°E, averaged between 10°N and 10°S for HadCM3-FA. The regressions of 850-hPa wind vectors onto the same base time series are superimposed. Data are only plotted at grid points where the local regression is significant at the 95% level. Fields are plotted at time intervals of 6 days, from (a) –18 to (h) +24 days, with (d) day 0 indicating the day of minimum 200-hPa VP at 90°E.

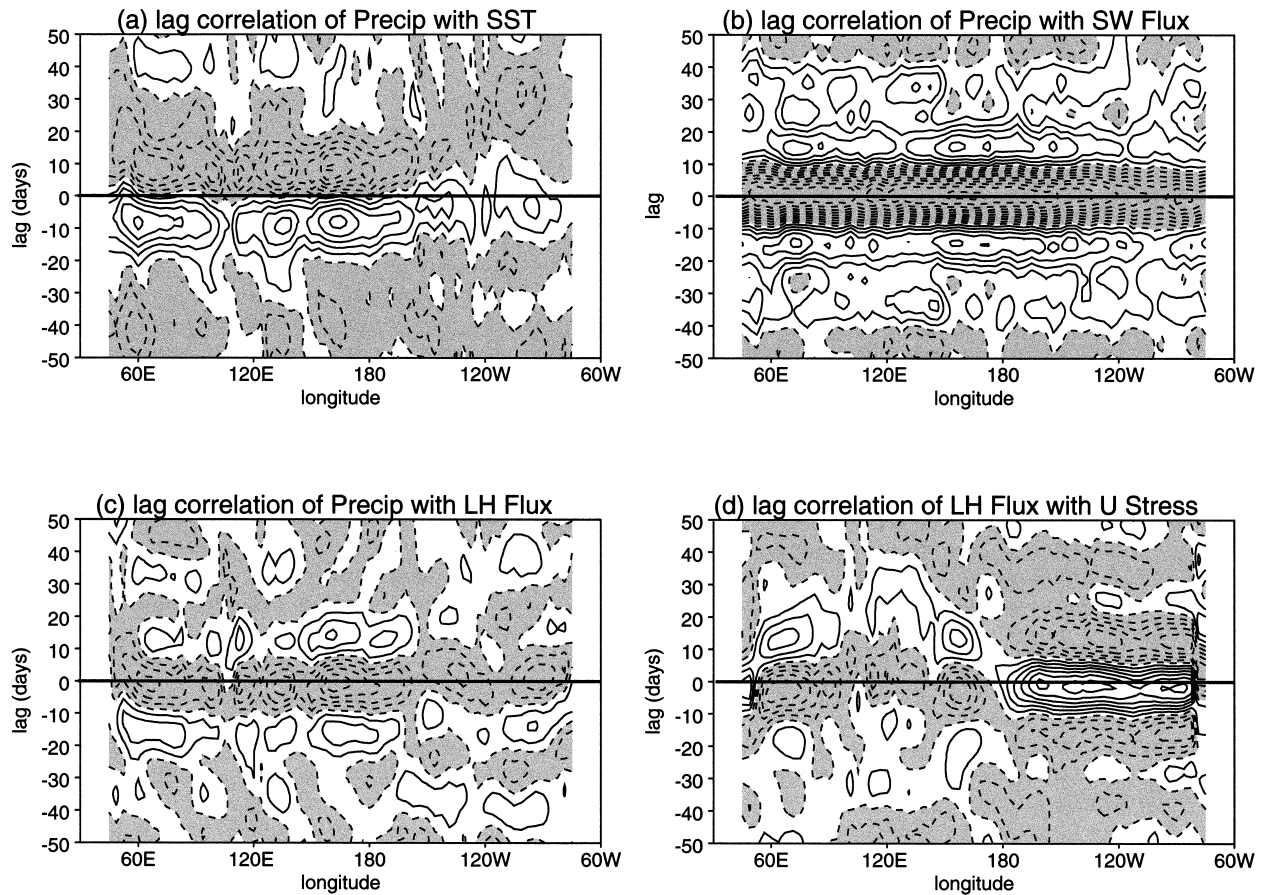


FIG. 9. (a) Lag correlation between convective precipitation and SST from HadCM3-FA. Negative lags indicate that SST leads precipitation. Positive correlations indicate that enhanced convection is correlated with a positive SST anomaly. Contour interval is 0.1 and negative correlation contours are dashed. Negative correlations are shaded. (b) Same as (a) but for convective precipitation and surface SWF. (c) Same as (a) but for convective precipitation and surface LHF. (d) Same as (a) but for LHF and UST. All fields are 20–100-day filtered and averaged between  $5^{\circ}\text{N}$  and  $5^{\circ}\text{S}$ .

of less than 0.3. However, in HadCM3-FA the strong lead–lag relationship is maintained as far east as  $160^{\circ}\text{W}$ .

The relationship between convective precipitation and surface SWF is indistinguishable between the two model versions, with enhanced convection being associated with reduced SWF at all longitudes at zero lag. This simply shows that the SWF reaching the surface is reduced when convection is enhanced in both versions of the model, an obvious relationship.

The relationship between convection and LHF is different between the two versions of the coupled GCM. In HadCM3, the negative correlation between convective precipitation and LHF breaks down to the east of  $140^{\circ}\text{E}$ , the same longitude at which the correlation between convective precipitation and SST also breaks down. In HadCM3-FA, the negative correlation between LHF and precipitation remains greater than  $-0.2$  to the east of the date line. The correlation between SST and convective precipitation also remains strong out to the date line. This suggests that it is a change in the LHF anomaly that is responsible for the change in the rela-

tionship between SST and convection between the two model versions.

Note that both HadCM3 and HadCM3-FA show a systematic shift in the location of the maximum evaporative cooling relative to the convective maximum when compared to the observed pattern. Both GCMs have the maximum negative correlation between LHF and convective precipitation close to lag zero whereas the observed pattern shows that the maximum in evaporative cooling lags the maximum in precipitation by about 5 days. This has been discussed in detail in section 4 of IS03. This seems to be a fundamental property of this particular atmospheric GCM, but it is possible that the real atmosphere behaves in this way too. Observations from a surface mooring in the west Pacific discussed by Zhang and McPhaden (2000) showed that the maximum in evaporative cooling of SST was coincident with the maximum in convective precipitation in a composite of 13 MJO episodes on the equator at  $165^{\circ}\text{E}$ .

HadCM3-FA shows a significant relationship between convection and LHF in the west Pacific that was not

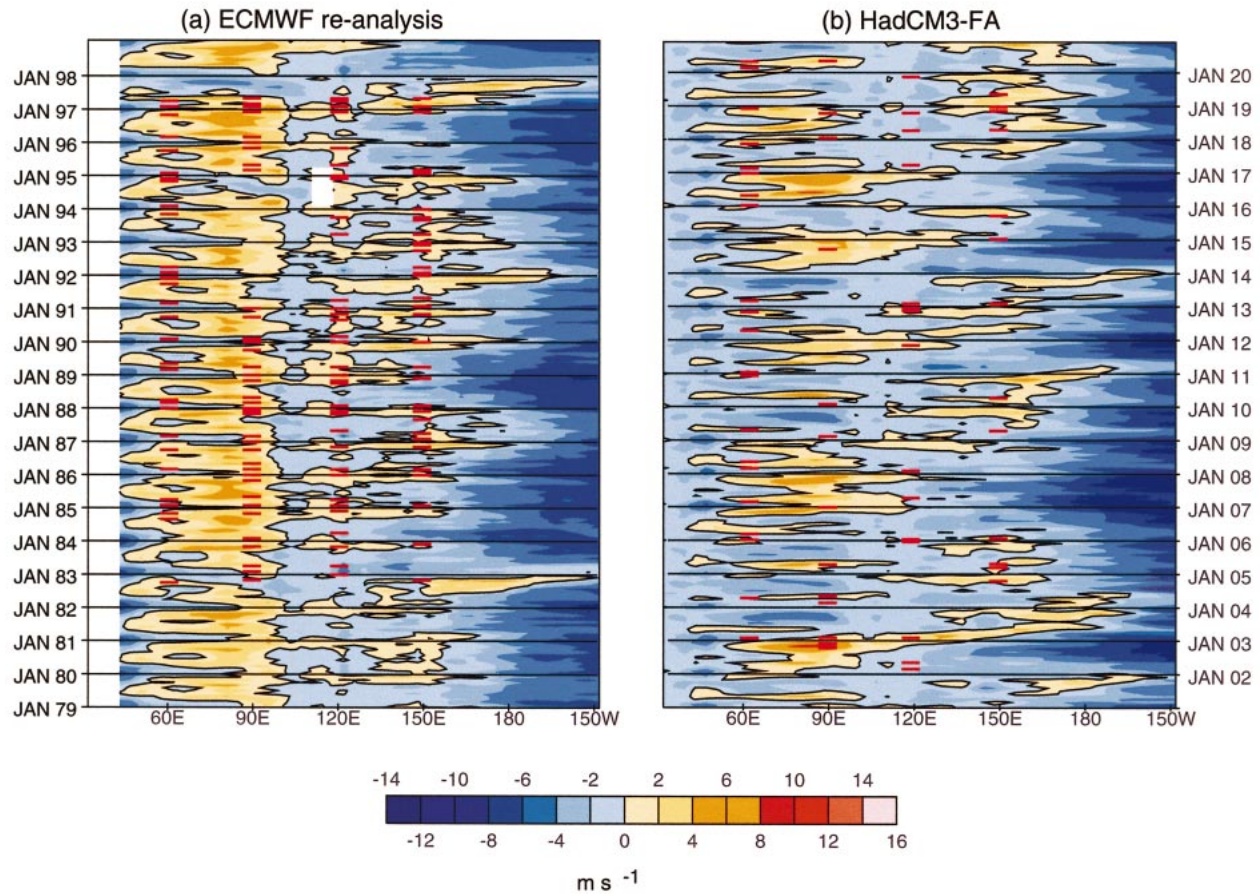


FIG. 10. Time-longitude plots of monthly mean zonal wind at 1000 hPa, averaged between  $4^{\circ}\text{N}$  and  $4^{\circ}\text{S}$  from (a) ECMWF reanalyses (1979–98) and (b) 20 yr of HadCM3-FA simulation. Red tick marks at  $60^{\circ}$ ,  $90^{\circ}$ ,  $120^{\circ}$ , and  $150^{\circ}\text{E}$  indicate the passage of the enhanced convection phase of the MJO through that longitude.

seen in HadCM3. However, the correlation between convection and LHF in HadCM3-FA is weak and less coherent in time around  $120^{\circ}\text{E}$ . The correlation between LHF and UST in HadCM3-FA around this longitude breaks down completely, as shown in Fig. 9d. In the observations, however, there is a negative correlation out to the date line where the basic-state winds change sign (see Fig. 9d in IS03). In the standard version of HadCM3, UST, and LHF are strongly negatively correlated between  $60^{\circ}$  and  $140^{\circ}\text{E}$  where the basic-state wind is a strong westerly. The correlation then changes sign abruptly and remains positive to the east of  $140^{\circ}\text{E}$  where the mean low-level zonal wind is easterly. In HadCM3-FA, the correlation is rather weak between  $100^{\circ}$  and  $150^{\circ}\text{E}$ . In this region, the mean low-level wind in ONDJFMA is a weak westerly (see Fig. 4). However, the seasonal mean picture masks the fact that there is a fair degree of variability in the strength and even the sign of the zonal wind in this region in HadCM3-FA. The weak westerly in the seasonal mean is made up from periods of westerlies interspersed with periods, sometimes lasting several months, when the wind becomes a light easterly. During the periods of easterlies,

or even near-zero winds, zonal wind anomalies such as those associated with the MJO can induce LHF anomalies of the opposite sign to those induced when the basic-state wind is westerly. Hence the correlation between UST and LHF over the entire period of the integration is weak.

This issue of the background wind being very light or even easterly so that the LHF anomalies induced by zonal wind stress anomalies may be of the wrong sign, is worth further investigation. Time-longitude plots of equatorial zonal wind at 1000 hPa from ERA and from HadCM3-FA are shown in Fig. 10. In the ERA data, the winds in the eastern Indian Ocean remain westerly almost all the time except in strong El Niño years such as 1982 and 1997. This is also the case in the standard version of HadCM3 (see Fig. 12b in IS03). In HadCM3-FA there is much more (unrealistic) variability of the monthly mean low level wind in the Indian Ocean sector between westerlies and easterlies and there are periods of many months when the wind is continuously easterly. On the other hand, the extension of westerly flow out to the date line also shows a large degree of variability

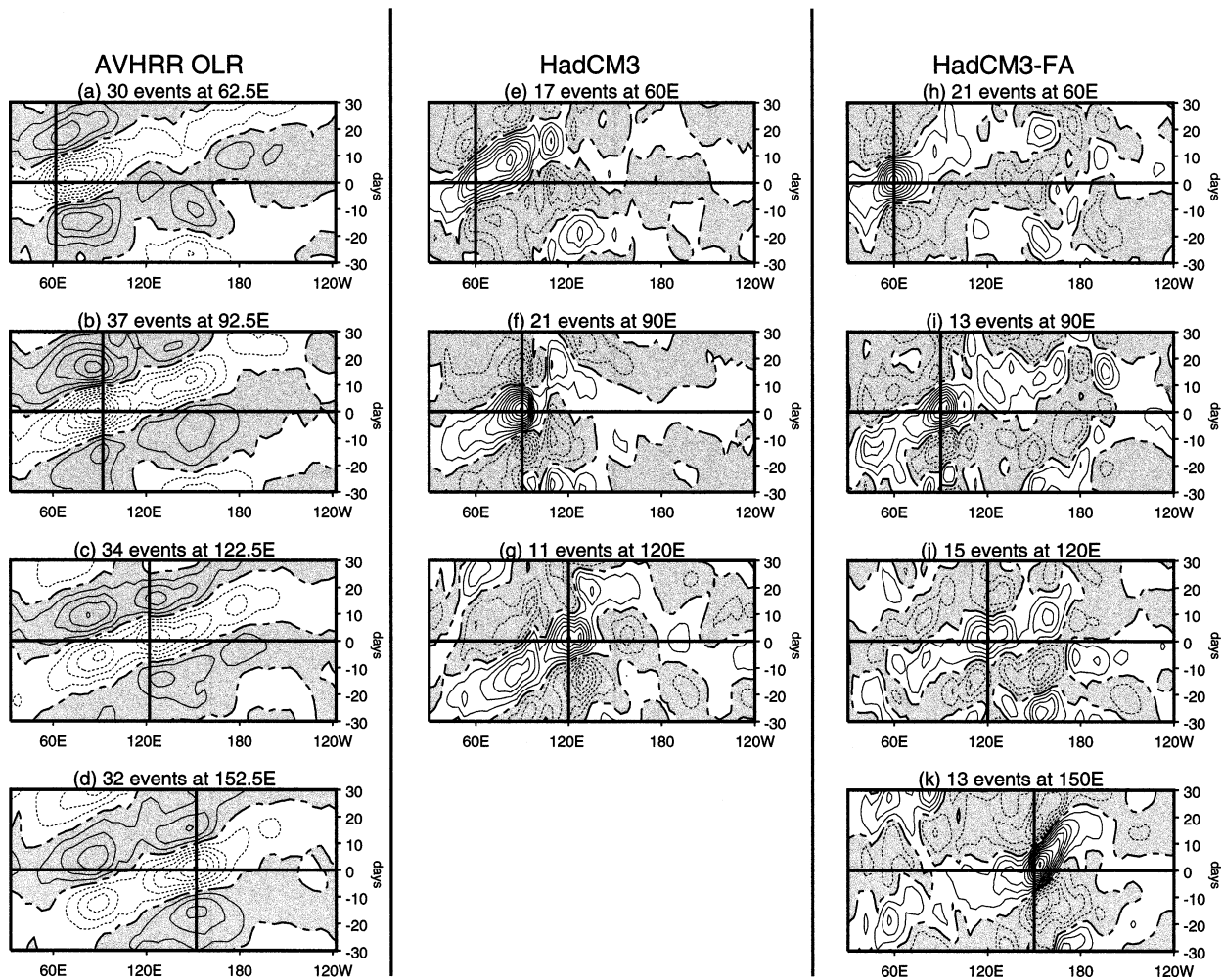


FIG. 11. Time-longitude composites of OLR or convective precipitation anomaly based on eastward propagating convective events at  $60^{\circ}$ ,  $90^{\circ}$ ,  $120^{\circ}$ , and  $150^{\circ}$ E: (a)–(d) NOAA AVHRR OLR, (e)–(g) HadCM3, and (h)–(k) HadCM3-FA. Contour interval is  $5 \text{ W m}^{-2}$  for OLR and  $0.5 \text{ mm day}^{-1}$  for precipitation. Positive OLR anomalies and negative precipitation anomalies are shaded.

but this compares quite well to the pattern seen in re-analysis fields.

The weakening and frequent reversal of westerly winds over the Indian Ocean in HadCM3-FA is an undesirable result of the flux adjustment. This may be due to the fact that the main convective region has shifted to the east, from the Maritime Continent into the west Pacific. It is also possible that the slight reduction in SST gradient on the eastern side of the Indian Ocean (see Fig. 2) results in weaker low-level westerly flow in this region.

If the coupled mechanism for the eastward propagation is the sole reason for the maintenance of the MJO then we would expect to see eastward moving convective anomalies occurring only when the background low level winds are westerly. This suggests that there will be fewer eastward propagating MJO events in the Indian Ocean in HadCM3-FA than in the standard version of HadCM3 because the periods of easterly winds will act

as a barrier to eastward propagation. However, because there are now periods when the mean wind is westerly in the west Pacific in HadCM3-FA, there may also be more MJO events extending to the east of the Maritime Continent in this version. This will be examined in the next section.

#### b. MJO events and the background zonal wind

In IS03, individual MJO events were identified at 4 different longitudes in observed OLR data, HadCM3, and HadAM3. These events were then used to produce MJO composites at each of the longitudes. The selection criteria were those of Woolnough et al. (2000), slightly modified, and are described in detail in IS03 section 3c. This analysis has been repeated for HadCM3-FA. Base points are located at  $60^{\circ}$ ,  $90^{\circ}$ ,  $120^{\circ}$ , and  $150^{\circ}$ E. Only events during ONDJFMA are included in this analysis. The number of eastward propagating convective events

TABLE 1. Summary of the number of eastward propagating convective events that occurred during Oct–Apr at four selected longitudes in observed OLR and convective precipitation from the standard and flux-adjusted coupled GCMs. Events are also stratified by the sign of the monthly mean zonal wind at the base longitude at the time of occurrence.

Method	No. of eastward propagating events at each base longitude			
	60°E	90°E	120°E	150°E
AVHRR OLR (16 yr)	30	37	34	32
(westerly:easterly)	(23:7)	(35:2)	(24:10)	(24:8)
HadCM3 (19 yr)	17	21	11	3
(westerly:easterly)	(14:3)	(21:0)	(5:6)	(0:3)
HadCM3-FA (19 yr)	21	13	15	13
(westerly:easterly)	(15:6)	(10:3)	(4:11)	(8:5)

during 19 yr of integration of HadCM3-FA at each of the four longitudes is shown in Table 1, together with the same figures for 19 yr of the standard version of HadCM3 and 16 yr of NOAA AVHRR observed OLR. The events have also been plotted as tick marks on Fig. 10 so that the sign of the basic-state zonal wind at the time of occurrence can be assessed.

At 60°E there are 21 events in HadCM3-FA, compared with 17 events at HadCM3. However, at 90°E, there are fewer events in HadCM3-FA than in the standard version of HadCM3. This suggests that, although a larger number of events initiate in the western Indian Ocean in HadCM3-FA, they tend not to propagate eastward as far as those identified in HadCM3. This would seem to be largely a result of the extended periods of easterly winds in the eastern Indian Ocean in HadCM3-FA, seen in Fig. 10b, which would act as a barrier to eastward propagation. Of the 13 events at 90°E in HadCM3-FA, 10 occur during periods when the mean wind in the eastern Indian Ocean is westerly. Thus, it appears that the weakening and frequent reversal of the mean zonal wind in the Indian Ocean in HadCM3-FA acts to reduce the number of MJO events in this basin and limits the eastward propagation of those that do occur.

At 120°E, both HadCM3 and HadCM3-FA produce similar numbers of eastward propagating events (11 and 15, respectively) which divide fairly evenly between periods of background easterlies and westerlies. As discussed in IS03, the coupled mechanism for the eastward propagation of the MJO may be less important at longitudes through the Maritime Continent due to the island landmasses. This issue will be further discussed in section 6.

Finally, HadCM3-FA produces 13 eastward propagating convective events at 150°E compared with only 3 in HadCM3. Of these 13, 8 occur during periods of westerly low-level winds. The increase in events in HadCM3-FA may be due either to the increased occurrence of mean westerly winds at this longitude, the increased SSTs due to the flux adjustment or some other factor. However, the fact that the atmosphere-only GCM,

HadAM3, has the correct SSTs in this region but only produces five rather weak and incoherent MJO events during 16 yr of integration, suggests that the coupled mechanism for maintaining eastward propagation is playing an important role in the simulation of the MJO. This coupled mechanism is, in turn, dependent on the correct simulation of the mean low-level zonal wind. The reduction in the number of MJO events in the eastern Indian Ocean in HadCM3-FA, a negative result of this experiment, also appears to be linked to a change in the basic-state zonal wind rather than any change in the absolute values of SST.

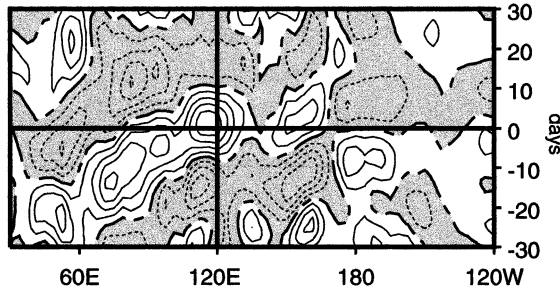
### c. Composite MJO events

As in IS03, the individual MJO events which have been identified can be used to form composites at the 4 base longitudes. The composites of convective precipitation from HadCM3-FA, together with those from HadCM3 and the composites from the NOAA satellite OLR dataset are shown in Fig. 11.

The composites of events at 60°E confirm the tentative conclusion drawn in the previous section that some of the MJO events in the western Indian Ocean in HadCM3-FA weaken or die out as they cross the basin due to the extended periods of easterly winds. The HadCM3-FA composite at this longitude is very strongly dominated by a standing oscillation with only weak propagation to the east, whereas in HadCM3, the composite shows much clearer eastward propagation across the whole of the Indian Ocean. A similar picture is obtained by looking at the composite at 90°E. Both coupled model versions have a strong standing component at this longitude, but in HadCM3 there is a stronger upstream signal indicating events propagating into this longitude from the west.

At 120°E, the HadCM3-FA composite shows an extension of enhanced convective precipitation into the west Pacific which is not seen in the standard HadCM3 composite at this longitude. However, both the signal in the Indian Ocean and that in the west Pacific are rather weak in HadCM3-FA for this base longitude when compared with the strength of the signal in the Indian Ocean in HadCM3. Closer examination of the events identified at 120°E in HadCM3-FA reveals that they fall into three classes. Of the 15 events at this longitude, 7 events originate in the Indian Ocean and propagate as far as the Maritime Continent but die out just to the east of 120°E; while 5 events originate over the Maritime Continent, just to the west of 120°E and propagate into the west Pacific. The remaining three events initiate in the Indian Ocean and propagate right across the Maritime Continent into the west Pacific. Thus very few events propagate all the way from the Indian Ocean to west Pacific in HadCM3-FA. So in the composite, the signal over the Indian Ocean will be weakened by the inclusion of events which initiate farther to the east, and the signal over the west Pacific will be weakened by

## (a) 10 Indian Ocean/Indonesia events at 120°E



## (b) 8 Indonesia/West Pacific events at 120°E

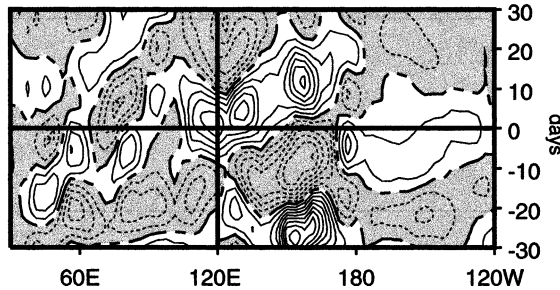


FIG. 12. Time-longitude composites of convective precipitation anomaly from HadCM3-FA based on (a) 10 eastward propagating convective events at 120°E, which initiate in the Indian Ocean and die out over Indonesia; and (b) 8 eastward propagating events at 120°E, which initiate over Indonesia and propagate into the west Pacific. Contour interval is 0.5 mm day<sup>-1</sup>.

the inclusion of events that have died out farther to the west. In the observations, of the 34 events at 122.5°E, 24 originate in the Indian Ocean and propagate into the west Pacific, 6 observed events initiate in the Indian Ocean and die out over Indonesia, and 4 events originate over Indonesia and propagate into the west Pacific.

In Fig. 12, composites are shown based on the Indian Ocean events and the west Pacific events in HadCM3-FA separately. The three events that propagate from Indian Ocean to west Pacific have been included in both composites. The composite precipitation events now look stronger in both ocean basins but the need to produce two composites at this longitude raises an important issue. It appears that the Maritime Continent itself acts as some sort of barrier to eastward propagation of convection in this model. This will be discussed further in section 6.

Finally, the HadCM3-FA composite at 150°E shows a very strong and rather slow moving disturbance, which appears to originate over the Maritime Continent and extends to the date line. The upstream extension of this feature into the Indian Ocean is rather weak, confirming that the Maritime Continent seems to act as something of a barrier to MJO events in this model, with rather few events propagating all the way from the Indian Ocean to the west Pacific. There is no composite at this longitude for the standard version of HadCM3 because there are only three eastward propagating events identified in this version.

More eastward propagating events are identified over Indonesia and the west Pacific in HadCM3-FA than in HadCM3, indicating that the change in the basic state in this region is important for the simulation of the MJO. However, the fact that there are still fewer events than are observed, and those events that the model does produce are somewhat weak and less spatially coherent than observed, suggests that there is still a fundamental problem with the representation of the large-scale organization of convection in this GCM.

The composites of SST corresponding to the precipitation composites are shown in Fig. 13. The composites for HadCM3-FA show SST anomalies which are very weak in the Indian Ocean compared to observations and HadCM3, and show no sign of propagation. However, the composite at 150°E for HadCM3-FA shows anomalies that are of about the same magnitude as in observations, and that propagate eastward. The coupling between convection and SST seems to be very weak in the Indian Ocean and Maritime Continent sector in HadCM3-FA. This is most likely to be due to the weakening or reversal of the mean low-level westerly wind here, so that wind anomalies induced by the MJO do not produce LHF anomalies of the correct sign. This will weaken the eastward propagation of the convection. It is also possible that the flux adjustment itself may be interfering with the intraseasonal SST variability in this basin, although the magnitude of the flux adjustment terms in the Indian Ocean is very small, with very little variation through the year.

The composite surface flux anomalies are shown in Fig. 14, with a positive flux anomaly defined as being into the surface. The flux anomaly is actually the sum of the LHF and the SWF as both the longwave and sensible heat flux anomalies are negligible compared to these two components. Over the Indian Ocean, the composite surface flux anomalies in HadCM3-FA are generally 4–8 W m<sup>-2</sup> weaker than in HadCM3. Examination of the individual components of the flux anomaly indicates that it is the LHF component that leads to this difference. Because of the variability between easterly and westerly winds in the Indian Ocean, and the periods when the mean wind is close to zero, the zonal wind stress anomalies associated with regions of enhanced convection can sometimes lead to LHF anomalies which are of the opposite sign to what would be expected if the background wind was westerly and of larger magnitude than the wind anomaly.

## 5. Simulation of the MJO in a coupled model with warmer Pacific SSTs

The flux-adjusted experiment provides evidence that the extension of the MJO into the west Pacific is related to the basic state westerly winds between the Maritime Continent and the date line. However, there is still a possibility that it is the warming of the SSTs in this region by the flux adjustment, which is actually re-

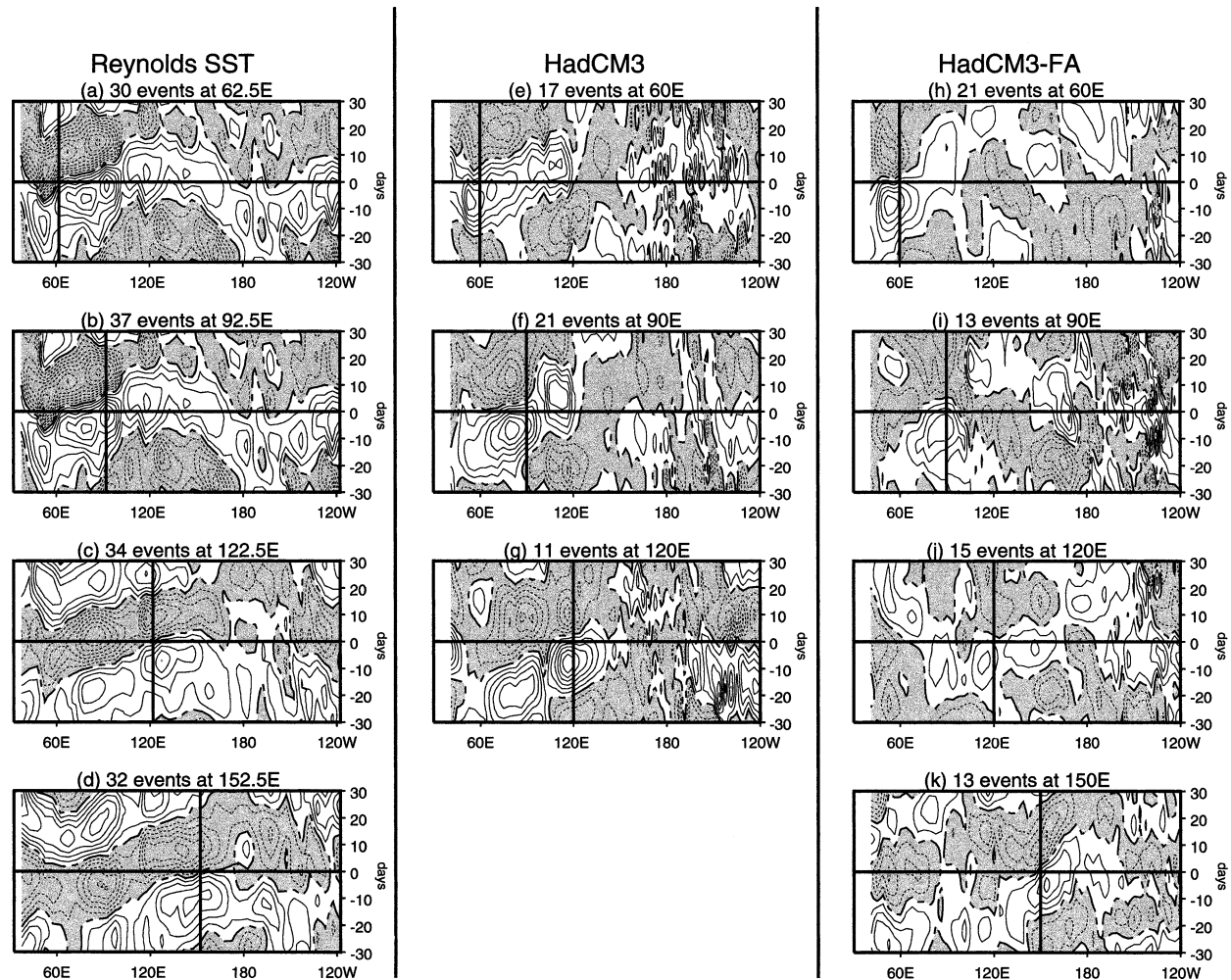


FIG. 13. Same as Fig. 11 except for SST anomalies: (a)–(d) Reynolds SST, (e)–(g) HadCM3, and (h)–(k) HadCM3-FA. Contour interval is  $0.025^{\circ}\text{C}$ . Negative anomalies are shaded.

responsible for the change in MJO behaviour. This remaining question can now be addressed by looking at a different coupled model configuration in which the ocean component of HadCM3 is replaced by a different ocean GCM. This coupled system predicts warmer SSTs throughout the Pacific Ocean, particularly in the equatorial cold tongue region, without the need for flux adjustment. The atmospheric component of the Hadley Centre GCM (HadAM3) has recently been coupled to OPA, the ocean model of the Laboratoire d’Oceanographie Dynamique et de Climatologie (LODYC). This ocean model has higher meridional resolution in the Tropics ( $0.5^{\circ}$  of latitude on the equator) than the ocean component of HadCM3 but the vertical resolution is similar to HadCM3 with 10 model levels in the top 100 m. The ocean physics of OPA, while being based on similar assumptions to HadCM3, differs in its precise formulation and implementation. Full details of the formulation of this ocean model can be found in Madec et al. (1998), and the version used in this

study has the same configuration and physics as described by Guilyardi et al. (2002, manuscript submitted to *J. Climate*). This coupled configuration of HadAM3 and OPA is known as HadOPA. A 20-yr segment of the control integration of this GCM has been analyzed for MJO-related variability.

HadOPA has a very similar basic-state climatology to HadCM3 in the tropical warm pool region, with similar SST gradients. However, the absolute values of SST are generally  $1^{\circ}$  to  $3^{\circ}\text{C}$  warmer, particularly in the equatorial cold tongue. Figure 15 shows the ONDJFMA climatologies of SST, precipitation and 850-hPa zonal wind for HadOPA. These can be compared with Figs. 2, 3, and 4 for the same fields from observations and the other coupled GCM configurations already described. Despite the increase in SST, the distribution of convective precipitation is similar to HadCM3, with the heaviest rain over Indonesia. The 850-hPa wind climatology is also very similar to HadCM3 with low-level westerlies over the equatorial Indian Ocean and

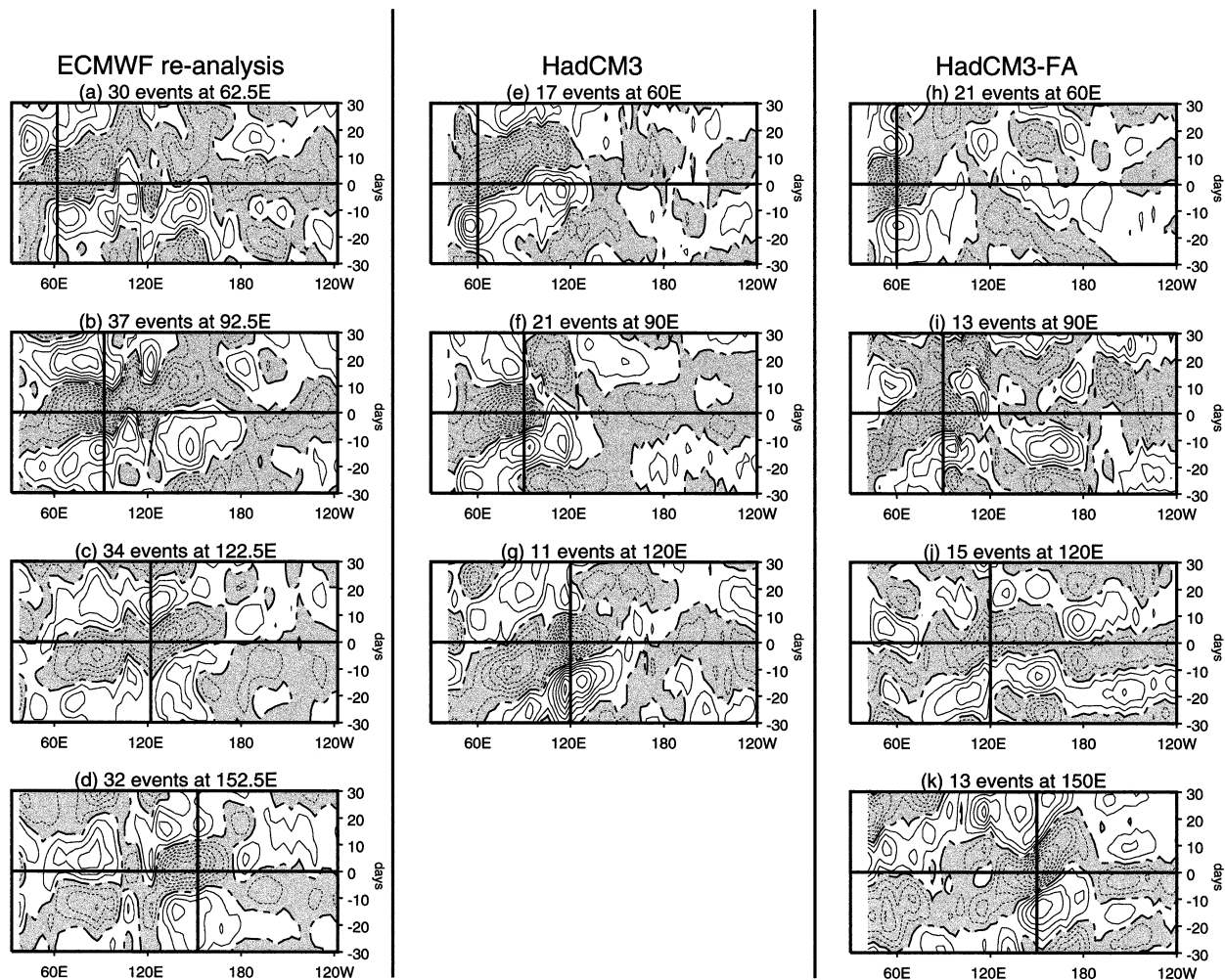


FIG. 14. Same as Fig. 11 except for surface anomalies (SWF + LHF): (a)–(d) ECMWF reanalysis, (e)–(g) HadCM3, and (h)–(k) HadCM3-FA. A positive flux anomaly is into the surface. Contour interval is  $4 \text{ W m}^{-2}$  and negative flux anomalies are shaded.

Maritime Continent, but not extending into the west Pacific. This coupled GCM, with an identical atmospheric model to HadCM3 but with warmer tropical SSTs, is therefore an ideal tool to study whether it is the lack of westerly winds or the cold SSTs which prevent the MJO extending into the west Pacific in HadCM3.

Figure 16 shows the lag correlation of convective precipitation averaged between  $5^{\circ}\text{N}$  and  $5^{\circ}\text{S}$  and the 200-hPa VP at  $90^{\circ}\text{E}$ , also averaged between  $5^{\circ}\text{N}$  and  $5^{\circ}\text{S}$ . It can be directly compared with the plots in Fig. 7, which show the same correlations from observations, HadCM3 and HadCM3-FA. The HadOPA picture is almost identical to that from HadCM3, with eastward propagation of convection across the Indian Ocean which comes to an abrupt halt at around  $120^{\circ}\text{E}$ . There is also some indication of an increase in convective activity in the central Pacific at the same time as the MJO convection peaks at around  $90^{\circ}\text{E}$ , but this is somewhat less marked than in HadCM3.

The spatial reconstruction of the MJO in HadOPA using the lag-regression technique described in IS03 is shown in Fig. 17. Like HadCM3, the development and propagation of the enhanced convective region in the Indian Ocean is quite realistic. However, as the convection approaches Indonesia it splits into two centers that propagate away from the equator, with a corresponding splitting of the westerly wind anomaly. Although the convective anomalies in HadOPA are slightly weaker than those seen in HadCM3, the patterns are very similar. So this coupled model provides further evidence that the lack of extension of the MJO into the west Pacific in HadCM3 is related to the lack of low-level westerly winds rather than the cold SSTs.

## 6. Discussion

A flux-adjusted coupled model integration has been performed in order to assess the impact of various model

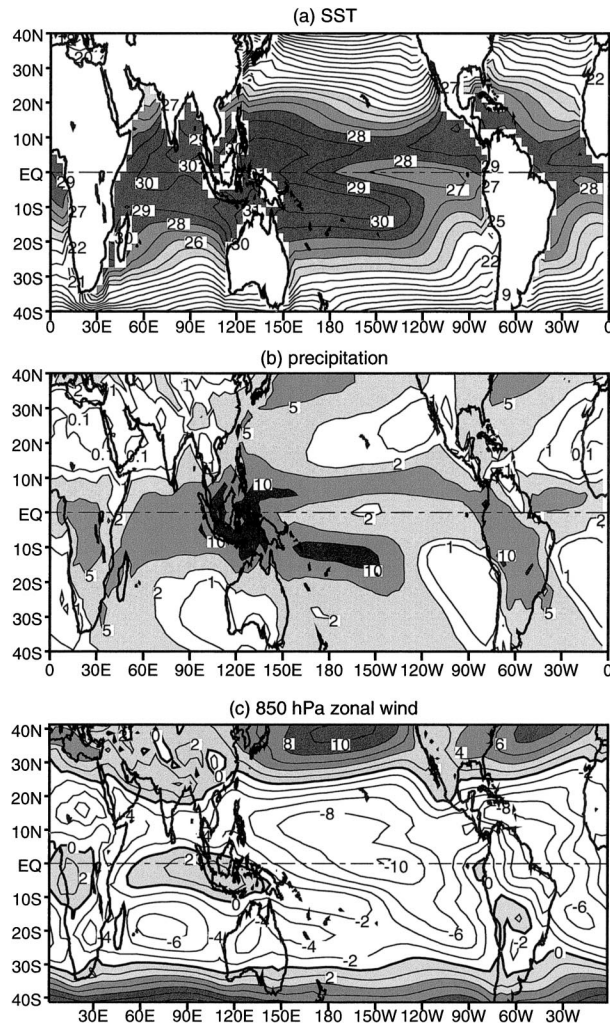


FIG. 15. Oct–Apr climatologies from 20 yr of HadOPA simulation for (a) SST (contour interval 1°C), (b) precipitation (contours at 0.1, 1.0, 2.0, 5.0, and 10.0 mm day<sup>-1</sup>), and (c) 850-hPa zonal wind (contour interval 2 m s<sup>-1</sup>). Regions with westerly winds are shaded.

systematic errors on the MJO simulation of a coupled GCM. The flux adjustment has been designed to warm the equatorial Pacific cold tongue and thus induce low-level westerly winds on and just to the south of the equator in the west Pacific. The flux-adjusted version of the GCM simulates MJO propagation into the West Pacific, which was not present in the standard version of the coupled GCM. However, the MJO in the Indian Ocean basin is weaker and occurs less often in the flux-adjusted version. MJO events do originate on the western side of the Indian Ocean basin, but many appear to break down as they cross the basin. This detrimental change in the MJO simulation by HadCM3-FA also appears to be due to a change in the basic-state zonal winds in this basin.

The flux adjustments to HadCM3-FA result in a low-level wind climatology in the equatorial west Pacific which is closer to the observed pattern than the same

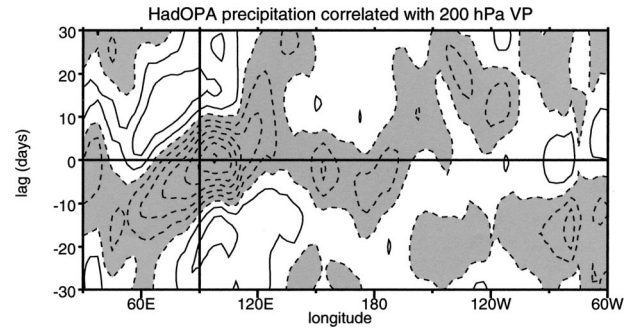


FIG. 16. Same as Fig. 7b except for HadOPA.

coupled model with no flux adjustment. Mean westerly winds extend eastward from the Maritime Continent to the date line between the equator and 10°S, while in HadCM3 the winds in this region are easterly throughout the 20-yr integration. The air–sea coupled intraseasonal interaction (ASCII) mechanism for the MJO, proposed by Flatau et al. (1997) requires that the low-level winds should be westerly for the coupling between convection and SST to maintain the MJO. The extension of the MJO into the west Pacific in HadCM3-FA would seem to provide corroborating evidence for this theory. At the same time, the mean westerly winds in the Indian Ocean are weakened in HadCM3-FA and sometimes become easterly for extended periods. This behavior is not seen in observations or in the standard version of HadCM3 except during strong ENSO warm events. The MJO in this basin is also weaker and less frequent in HadCM3-FA, which again would be expected if the coupled mechanism is operating.

Some eastward propagating events occur in both versions of the coupled model during periods of mean low-level easterly winds. However, these are less frequent and weaker than the events that occur during periods of mean westerlies. This suggests that the coupled mechanism is not the sole reason for the eastward propagation of convection, but instead acts as an amplifying mechanism for existing eastward propagating atmospheric disturbances. This is consistent with IS03, which showed that the atmosphere-only GCM, HadAM3, was able to produce eastward moving convective events but these events were rather weak. Other studies of the MJO in atmosphere-only GCMs (e.g., Slingo et al. 1996) have also shown that such GCMs can produce eastward moving disturbances but that these generally tend to be weak and rather incoherent. Neither HadCM3 or HadCM3-FA simulate as many MJO events as are actually observed. This suggests that there is still much scope for improving the simulation of tropical intraseasonal variability in this GCM.

In both HadCM3 and HadCM3-FA, the magnitude of the MJO-related SST anomalies is smaller than observed although the surface flux anomalies associated with the MJO are of about the right magnitude. This suggests that the ocean mixed layer representation in the GCM

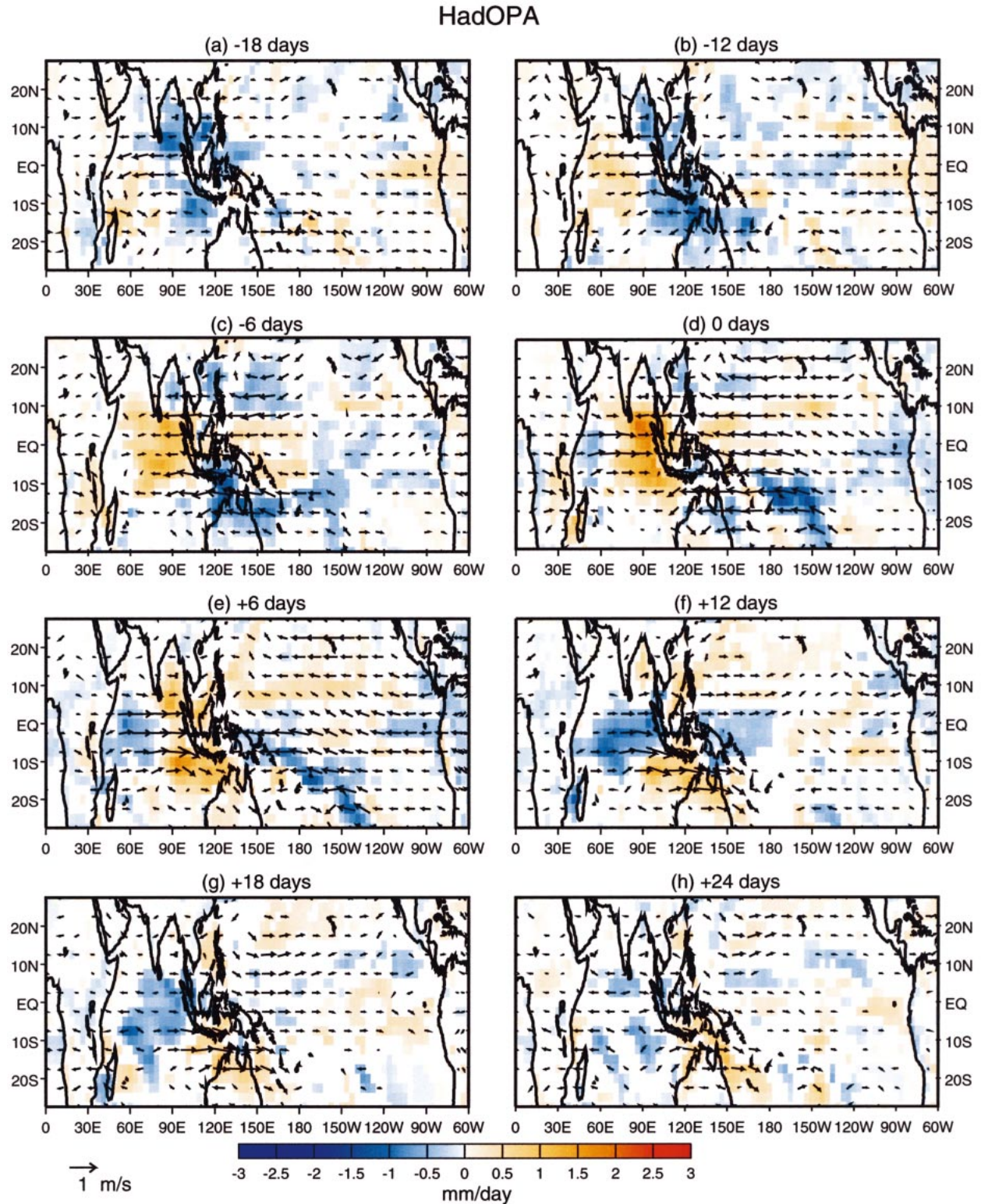


FIG. 17. Same as Fig. 8 except for HadOPA.

may be too coarse. Studies of the upper ocean in the warm pool region such as that of Weller and Anderson (1996) have shown that, during the clear sky/light wind phase of the MJO, the mixed layer becomes very shallow and there can be large variations of SST ( $1^{\circ}\text{C}$ ) on diurnal timescales. It is hypothesized by Slingo et al. (2003, hereafter SINWY) that such diurnal changes in SST may contribute to the forcing of convection of a cumulus congestus type which may itself be an important component of the MJO cycle, recharging the moisture of the free troposphere during the suppressed phase (Johnson et al. 1999). In order to capture this variability, SINWY suggest that the ocean mixed layer will need to have sufficiently high resolution to represent the detailed structures which are observed. Coupling between the ocean and atmosphere also needs to occur more often than once per day, the coupling frequency used in HadCM3 and HadCM3-FA. The findings of Shinoda and Hendon (1998) support this argument. They show that including diurnal variations of surface fluxes in a mixed layer model of the tropical west Pacific leads to larger intraseasonal SST variations associated with the MJO. The diurnal enhancement was largest during the suppressed phase of the MJO.

In the standard version of HadCM3, the SSTs in the equatorial west Pacific region are too cold by  $1^{\circ}$  to  $2^{\circ}\text{C}$  throughout ONDJFMA. It is possible that the lack of extension of the MJO into this region is due to the cold SSTs rather than the lack of westerly winds. HadCM3-FA has warmer SSTs in this region as well as having westerly winds, so it could be that the extension of the MJO into the west Pacific in this version of the model was due to the warmer (and thus more realistic) SSTs rather than the improved wind climatology. There are several strands of evidence which suggest that this is not the case. First, it was shown in IS03 that the atmosphere-only version of this model, forced with observed SSTs did not produce a coherent MJO signal. This suggests that coupling to an ocean surface is necessary for a good simulation of the MJO. Second, the differences in MJO simulation in the Indian Ocean between HadCM3 and HadCM3-FA are most likely to be due to the changes in the wind climatology since the SSTs in this region do not change between the two versions, apart from a slight cooling in the east of the basin. Third, the atmospheric component of HadCM3 has also been run coupled to a different ocean model, a configuration known as HadOPA. This model has an almost identical low-level wind climatology in the west Pacific to HadCM3, but the SSTs in the region are  $2^{\circ}\text{C}$  warmer. Despite the increase in SSTs, the MJO still does not propagate into the west Pacific indicating that the easterly low-level winds act as a barrier to eastward propagation of convection.

Both versions of the coupled GCM seem to have problems representing the propagation of the MJO through the Indonesian region. IS03 showed that, in the standard version of HadCM3, the convective maximum

tended to split into two centers as it approached Indonesia, moving away from the equator to the north and south. In HadCM3-FA, many of the convective events in the Indian Ocean appeared to die out over the Maritime Continent, although this region also appeared to be the source region for the majority of events which propagated across the west Pacific. Neale and Slingo (2003) have shown that the atmosphere-only version of this GCM has problems representing the mean climate of the Maritime Continent. They speculated that this may be due to the inability of the GCM convection, surface exchange and boundary layer parametrization schemes to represent the complex diurnal variations in convection around the Indonesian Islands which are very coarsely resolved in the model. It is possible that the intraseasonal variations in convection in this region are also affected by the same model shortcomings. It is certainly likely that the eastward propagation of MJO-enhanced convection through this region is not due entirely to the coupled mechanism of Flatau et al. (1997) simply because of the presence of the island landmasses. It may be that the intraseasonal variability associated with the MJO in this region results partially from an enhancement or suppression of the diurnal cycle of convection over and around the islands as the large-scale dynamics associated with the MJO convective region interact with the smaller-scale processes associated with the islands themselves. This aspect of tropical variability will be the subject of future work.

*Acknowledgments.* The authors acknowledge support through the NERC-funded UK Universities Global Atmospheric Modeling Programme. The HadOPA model was developed as part of a joint project between the NERC Centre for Global Atmospheric Modeling at the University of Reading, the Laboratoire d'Océanographie Dynamique et de Climatologie at the University of Paris 6 and the Met Office.

#### REFERENCES

- Flatau, M., P. Flatau, P. Phoebus, and P. Niiler, 1997: The feedback between equatorial convection and local radiative and evaporative processes: The implications for intraseasonal oscillations. *J. Atmos. Sci.*, **54**, 2373–2386.
- Gent, P., and J. C. McWilliams, 1990: Isopycnal mixing in ocean circulation models. *J. Phys. Oceanogr.*, **20**, 150–155.
- Gordon, C., C. Cooper, C. A. Senior, H. Banks, J. M. Gregory, T. C. Johns, J. F. B. Mitchell, and R. A. Wood, 2000: The simulation of SST, sea ice extents and ocean heat transports in a version of the Hadley Centre coupled model without flux adjustments. *Climate Dyn.*, **16**, 147–168.
- Gregory, D., and P. R. Rowntree, 1990: A mass flux convection scheme with representation of cloud ensemble characteristics and stability dependent closure. *Mon. Wea. Rev.*, **118**, 1483–1506.
- , R. Kershaw, and P. M. Inness, 1997: Parameterization of momentum transport by convection. II: Tests in single-column and general circulation models. *Quart. J. Roy. Meteor. Soc.*, **123**, 1153–1183.
- Hendon, H. H., 2000: Impact of air–sea coupling on the Madden–

- Julian Oscillation in a general circulation model. *J. Atmos. Sci.*, **57**, 3939–3952.
- , and J. Glick, 1997: Intraseasonal air–sea interaction in the tropical Indian and Pacific Oceans. *J. Climate*, **10**, 647–661.
- Inness, P. M., and J. M. Slingo, 2003: Simulation of the Madden–Julian Oscillation in a coupled general circulation model. Part I: Comparisons with observations and an atmosphere-only GCM. *J. Climate*, **16**, 345–364.
- , —, S. J. Woolnough, R. B. Neale, and V. D. Pope, 2001: Organization of tropical convection in a GCM with varying vertical resolution: Implications for the simulation of the Madden–Julian oscillation. *Climate Dyn.*, **17**, 777–793.
- Johnson, R. H., T. M. Rickenbach, S. A. Rutledge, P. E. Ciesielski, and W. H. Schubert, 1999: Trimodal characteristics of tropical convection. *J. Climate*, **12**, 2397–2418.
- Kraus, E. B., and J. S. Turner, 1967: A one dimensional model of the seasonal thermocline. II. The general theory and its consequences. *Tellus*, **19**, 98–105.
- Madec, G., P. Delecluse, M. Imbard, and C. Levy, 1998: OPA version 8.1 ocean general circulation model reference manual. Tech. Rep. 11, LODYC/IPSL, Jussieu University, Paris, France, 91 pp.
- Neale, R. B., and J. M. Slingo, 2003: The Maritime Continent and its role in the global climate: A GCM study. *J. Climate*, **16**, 834–848.
- Rayner, N. A., E. B. Horton, D. E. Parker, C. K. Folland, and R. B. Hackett, 1996: Version 2.2 of the global sea-ice and sea surface temperature data-set 1903–1994. Climate Research Tech. Note 74, Hadley Centre, Bracknell, United Kingdom, 35 pp.
- Shinoda, T., and H. H. Hendon, 1998: Mixed layer modelling of intraseasonal variability in the tropical western Pacific and Indian Oceans. *J. Climate*, **11**, 2668–2685.
- Slingo, J. M., and Coauthors, 1996: Intraseasonal oscillations in 15 atmospheric general circulation models: Results from an AMIP diagnostic subproject. *Climate Dyn.*, **12**, 325–357.
- , D. P. Rowell, K. R. Sperber, and F. Nortley, 1999: On the predictability of the interannual behaviour of the Madden–Julian oscillation and its relationship with El Niño. *Quart. J. Roy. Meteor. Soc.*, **125**, 583–609.
- , P. M. Inness, R. B. Neale, S. J. Woolnough, and G.-Y. Yang, 2003: Scale interactions on diurnal to seasonal timescales and their relevance to model systematic errors. *Ann. Geophys.*, in press.
- Waliser, D. E., K. M. Lau, and J.-H. Kim, 1999: The influence of coupled SSTs on the Madden–Julian oscillation: A model perturbation experiment. *J. Atmos. Sci.*, **56**, 333–358.
- Weller, R. A., and S. P. Anderson, 1996: Surface meteorology and air–sea fluxes in the western equatorial Pacific warm pool during the TOGA coupled ocean–atmosphere experiment. *J. Climate*, **9**, 1959–1990.
- Woolnough, S. J., J. M. Slingo, and B. J. Hoskins, 2000: The relationship between convection and sea surface temperature on intraseasonal timescales. *J. Climate*, **13**, 2086–2104.
- Xie, P., and P. A. Arkin, 1996: Analyses of global monthly precipitation using gauge observations satellite estimates, and numerical model predictions. *J. Climate*, **9**, 840–858.
- Zhang, C., and M. J. McPhaden, 2000: Intraseasonal surface cooling in the equatorial west Pacific. *J. Climate*, **13**, 2261–2276.